Case-Study on Visible Light Communication for Implant Monitoring

Maximilian Koschay*, Henryk Richter†, Meike Statz‡, Maria Kober‡, Jonas Puschmann,
Franz Plocksties*, Alexander Storch‡, Volker Kühn† and Dirk Timmermann*
* Institute of Applied Microelectronics and Computer Engineering, University of Rostock, 18119 Rostock, Germany
† Institute of Communications, University of Rostock, 18119 Rostock, Germany
‡ Department of Neurology, University Medical Center Rostock, 18147 Rostock, Germany

***Abstract*—The focus of this paper is the feasibility of Visible Light Communication (VLC) for the monitoring of implants in rodents by example of two approaches. One of the VLC variants is intended for manually triggered transmission and takes advantage of the CMOS sensor rolling shutter principle. The second approach is designed mainly for autonomous monitoring. Trials with freely moving animals have shown that the first approach provides a throughput of 148 bit/s. For the automatic monitoring a transmission every 6 hours is sufficient for a reliable daily update of the implant status.**

VLC exhibits limited range and channel capacity in comparison to radio frequency (RF) based telemetry. However, the advantage of VLC solutions is the minimal space requirement as only a single LED is needed in addition to the microcontroller on the transmitter side.

***Index Terms*—Visible Light Communication, Telemetry, Optical Camera Communication**

I. Introduction

Deep brain stimulation (DBS) is a neurological treatment option applying electrical high frequency stimulation (50-150 Hz dependent on application) through chronically implanted electrodes into specific brain structures [1]. In particular, it shows high efficacy in the treatment of motoric symptoms in movement disorders like Parkinson's Disease, Dystonia or Essential tremor [2]. Although DBS is a well-established therapeutic option, the underlying mechanisms are still controversial [1, 3]. Indeed, there is a number of side effects, including speech disorders, postural instability, apathy, depression, anxiety, impulse-control disorders, and even suicide [4, 5]. Additionally, the use of DBS for other neurological disorders, as depression, addiction, chronic pain or Tourette Syndrome is under investigation [1, 3, 6]. Thus, there is an urgent need for further research, in which DBS studies with animal models contribute significantly to the understanding and optimization of target regions and stimulation parameters in humans.

Subcutaneous implants as well as wireless and non-invasive telemetry enables stress-free animal experiments [7]. That means, the animals do not have to be restrained or anesthetized for the validation of implant functionalities. They are not restricted in their natural behavior, including group housing. This is not only important for animal welfare, it also enables behavior experiments, which are particularly necessary to investigate DBS effects on non-motor symptoms or psychiatric disorders [7, 8]. Data acquisition in regular intervals during the experimental timeline contribute to an optimized control of experimental studies.

State-of-the-art commercial neurostimulators [9] and implants from academia for animal studies [7] provide a wireless interface, which most often use radio frequency (RF) technology like Bluetooth or ZigBee. They provide sufficient throughput for the implant status and possibly additional sensor feedback. However, these systems increase the implant's size and energy requirements significantly, like in [10] in which the additional RF module nearly doubles the implant's volume. Both energy storage and implant size are very limiting constraints for the application in small animal models, such as rodents.

An alternative technology to RF is the unidirectional transmission of data over visible light. A great benefit of Visible Light Communication (VLC) is the minimal requirement of a single light source at the transmitter. Most implant devices that are used in animal studies provide one or more Status-LEDs for the user feedback, thus VLC comes at no additional cost of additional hardware. VLC protocols can also be designed to be of low complexity on the transmitter side.

In this work we evaluate the question if VLC is a usable alternative for small and infrequent data transmission from subcutaneous implants. We propose two different approaches to VLC receivers for two different application scenarios.

For our first approach the aim is to keep the hardware requirements in the laboratory as low as possible. For this we implemented a solution based on Optical Camera Communication (OCC). In OCC, the medical staff uses a smartphone camera to read the manually triggered LED signal from the device during the daily checkup routine of the animals. The approach and process are further explained in III.

The second approach to VLC-based implant monitoring aims to answer the question about the feasibility of unassisted transmission and data collection. The corresponding setup performs transmissions from the implant to a remote receiver in regular intervals for daily updates and is described in IV. We further present the results of animal studies for both approaches in V.

II. Transmitter device

To evaluate our two VLC methodologies for the application of implant status monitoring we utilize the STELLA neurostimulation device [7], which has been used in DBS animal studies on rats and hamsters. The device contains a 640 nm LED (Kingbright KPT-1609LVSECK-J3-PRV) that is driven by 2 mA at 3 V. The implant's TI MSP430G2553 microcontroller is programmed to control the LED's state according to the chosen signal modulation described in III and IV.

The implant is encapsulated with the methodology described in [10], although with a modified housing. The transparent encapsulation contains the electronics, the energy supplying CR1226 coin cell and was filled with epoxy resin (Polytec EP 601). The stimulation capabilities of the neurostimulator device have been disabled for the purpose of this study.

III. Manual Optical Camera Implant Communication

Common CMOS image sensors of smartphones use a rolling shutter, where the pixels are exposed and read out as consecutive rows. This characteristic can be exploited to increase the transmission throughput by flashing the LED at a frequency beyond the sensor frame rate [11]. The resulting stripe pattern from the rolling shutter effect (Fig. 1b) can be used to encode the data in the width and distance of the stripes.

We implemented an OCC system on the STELLA implant and a *Google Pixel 2* Android smartphone. The camera parameters were set as suggested in [12]. We utilized the recently published Android CameraX API and set the output to a 1200x1600 px image in the YCbCr 4:2:0 format at 30 frames per second.

In the various publications on OCC schemes, the transmitting sources range from room or object illuminating lights [11, 13, 14], pixel arrays [15, 16] to single- or multi-colored LEDs [12, 17]. In our application, the small red LED on the encapsulated implant under a layer of skin and fur results in a diffused light source with an illuminance of around 50 lx and a diameter of 20 mm. When capturing the transmitted signal with a camera, the light is only visible in a limited region of the image. Its position and size depend on the distance and orientation of the camera to the implant. Therefore, the first step of decoding the transmitted signal is to identify the region of interest (ROI) in each image [17]. The algorithm identifies the image column with the highest count of bright stripes, which is extracted from the Luma (Y) plane of the YCbCr buffer. Due to real-time constraints, the ROI width was limited and the chroma planes were disregarded. The result of the ROI extraction is a two-dimensional buffer of the ROI's Luma.

Most OCC solutions utilize an On-Off Keying Modulation, often additionally with Manchester encoded data to avoid flickering effects and to improve error detection [11, 12, 18]. We have decided to follow the suggestions made in the studies of Dudko et. al [17] and use Pulse Position Modulation (PPM) for a more reliable communication protocol. Since flickering of the light source is not an issue for our application and to keep

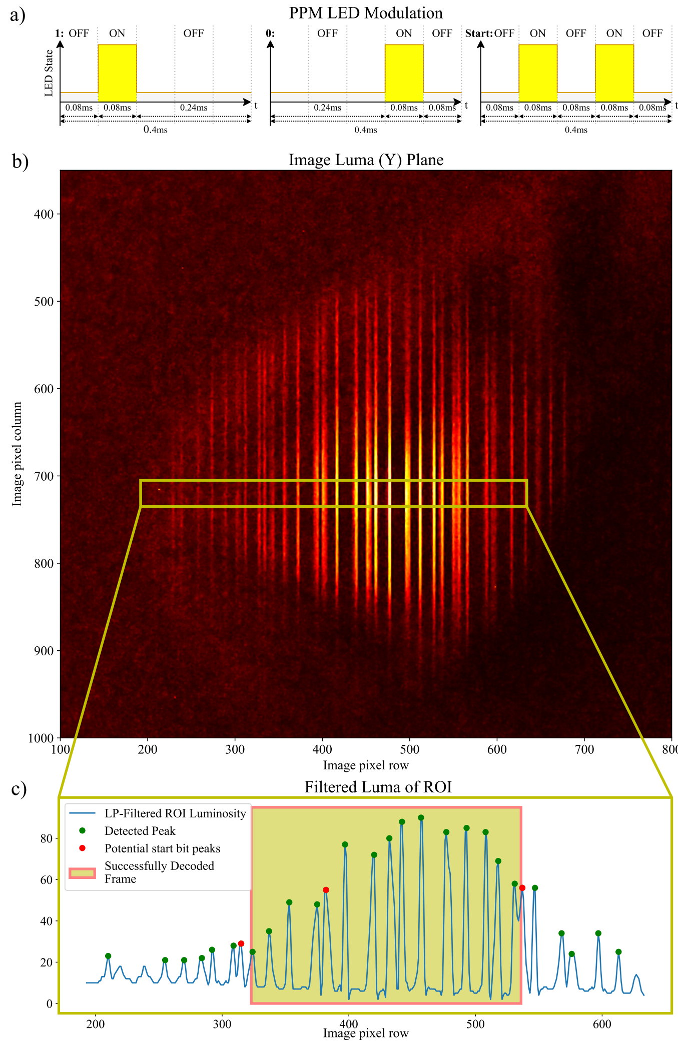

Fig. 1. (a) PPM Modulation of LED Signal, (b) Image Lumen and detected Region Of Interest, (c) Filtered Lumen of ROI and detected packet

the data size of the transmission as low as possible, we decided to not use any run length limited encoding. The duration of a PPM symbol was set to 0.4 ms. The symbols '1' and '0' are encoded by setting a single LED On-state of 0.08 ms at different positions during the symbol period, as visualized in Fig. 1a. Moreover, a synchronization symbol can be defined which removes the necessity of a synchronization sequence over multiple symbols [17].

Since the width of the bright and dark stripes in the image are proportional to the PPM symbol intervals, the ROI signal can be demodulated by the distance between LED On-State sequences [17]. In our implementation, we first detect the peaks by gradient detection over a short moving average window. The distances between the peaks are then sequentially correlated to the known PPM distances (Fig. 1c).

Since OCC is a frame discrete sampling scheme, the total payload must be split into packets [17]. The usable packet size depends on the data size as well as camera constraints and environmental factors. After experimental variations of these parameters, a compromise was found at a packet size of 15 bits for an exemplary total payload of 32 byte. One packet consists of the start symbol, five bits for the packet number, and one bit for a parity checksum of the complete packet.

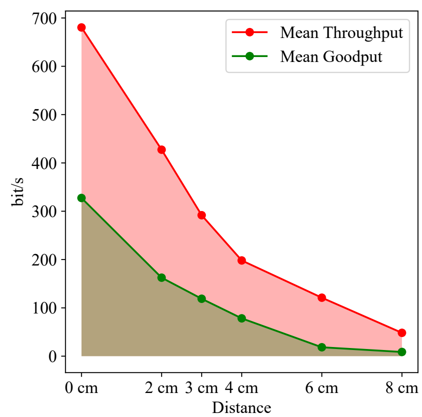

Fig. 2. Throughput and Goodput at distances between 0 to 8 cm

Fig. 2 shows the mean and maximum throughput as well as goodput over the distance between sensor and implant. They were measured on a stationary setup in which the sensor is placed in a direct line of sight, in a lighting environment similar to the conditions of the animal housing laboratory. The throughput is measured by counting the number of valid data bits received within one second. This also includes packets that have been received multiple times within a second, but excludes any packets with wrong payloads and failed parity checks. The goodput is defined as the time until all packets have been received successfully. On average 0.2% of the packets failed the parity test and only 0.06% wrongly decoded payloads were not detected by the parity test.

IV. Automated VLC Implant Monitoring

The unassisted implant monitoring approach is based on a stationary receiver and regular transmission of a binary frequency shift keying (FSK) modulated signal over the LED of the implant. The sent frame layout consists of a B13 barker code preamble, followed by the implant ID, the individual measurements, status codes and provisions for a concluding CRC-16. A 1/2 rate convolutional code with the polynomials [171;133] was applied on all data after the preamble for further error protection and correction.

The analog part of the experimental receiver consists of two hardware units in front of the analog to digital converter (ADC): a set of photo diodes alongside an impedance converter and a bandpass amplifier circuit (Fig. 3). The resulting signal was captured using a USB sound card at a rate of 48 kHz.

Given the signal $y[n]$ with the sampling rate f_a from the ADC on the receiver side, low complexity demodulation of the individual binary FSK components $y_0[n]$ and $y_1[n]$ corre-

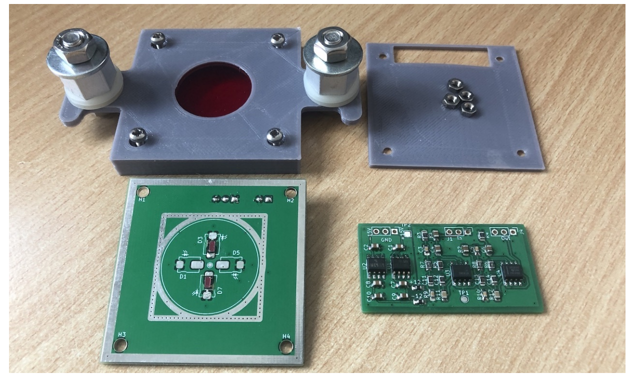

Fig. 3. Receiver frontend (l) and bandpass amplifier/filter (r)

sponding to the frequencies f_0 and f_1 can be accomplished by direct mixing.

$$y_\xi[n] = y[n] \cdot e^{-j2\pi n f_\xi / f_a} \quad \text{with } \xi \in [0, 1] \tag{1}$$

This step only requires one complex multiplication per FSK component and sample. The demodulation itself consists of moving average filtering on both streams $y_\xi[n]$, followed by the hard decision.

$$b[n] = \arg \max_{\xi=0,1} \left| y_\xi[n] * \mathrm{rect}_N[n] \right| \tag{2}$$

The moving average filter length N depends on the ratio between sampling rate and symbol rate. The remaining operation steps consist of preamble detection, downsampling of $b[n]$ and Viterbi decoding [19].

V. In-Vivo Animal Studies

We evaluated both VLC methodologies from III and IV on two male adult wild-type Wistar-Han rats (Charles River Laboratories, Sulzfeld, Germany). Both animals were implanted a STELLA neurostimulation device subcutaneously, placed between hip, costal arch and spine contralateral to the stimulation side (Figure 5b)[7]. The rats were housed under controlled conditions (12 h dark and light cycle, food and water ad libitum) in a group of two per cage. All animal experiments were conducted in accordance with European guidelines (2010/63/EU) and permitted by the local animal care committee (Landesamt für Landwirtschaft, Lebensmittelsicherheit und Fischerei, Mecklenburg-Vorpommern, Germany; LALLF M-V/7221.3-2-011/21).

A. Manual VLC capture using OCC

We tested the OCC system during the daily health check routine. The camera sensor was attempted to be held orthogonally 5 to 0 cm above the implants of the freely moving animals for 15 - 60 seconds after manual transmitter activation. Due to the movement of the animals on average only 52% of all frames of nine recordings contained identifiable ROIs. This reduced the mean throughput to 148 bit/s.

In our application it proved to be advantageous to set the packet parameters for a maximum throughput at the sacrifice of a short maximum distance, due to the placement of the

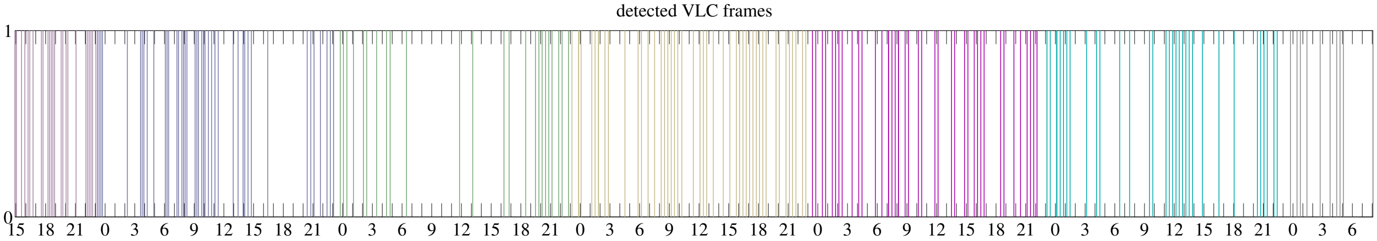

Fig. 4. Detected VLC frames during the 138 hour laboratory trial as vertical bars, denoted with different colors for each day

implant and the limited direct line of sight. The results of the animal studies suggest a good usability of this VLC method for manual implant status readouts. However, the chosen total payload size converges to the practical limit with an average required capture time of 8 seconds.

B. Automated VLC Monitoring

A laboratory trial was conducted over the period of one week observing the pair of animals in a cage (M3H, ZoonLab, 425x265x180 mm³) where the receiver was mounted on the upper part of the box facing diagonally down. As system parameters, a rate of 400 symbols/s, a frequency pair of 6.4/8 kHz and an interval of 20 minutes between sent frames were set for the implants in both rats. The observed signals were captured at 48 kHz sampling rate and stored for post analysis.

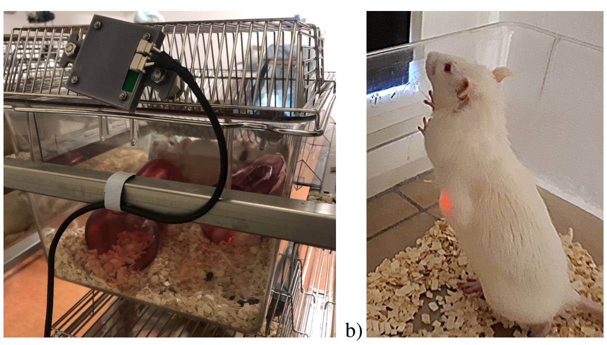

Fig. 5. a) Receiver frontend mounted to cage, b) Blinking implant in rat

Fig. 4 depicts the VLC frames that could be detected over the trial period. On the second and third day (blue, green), the cages were equipped with one opaque sleeping rolls instead of two red semi-transparent rolls shown in Fig. 5a. Within the last 24 hours of the trial, one of the transmitters went offline. Out of the total of 828 frames that should have been sent out over the trial of 138 hours by the implants, 213 frames were detected within the resulting data set. 176 bit per frame were kept constant across the trial to obtain the bit and frame error estimates of 13% and 33%, respectively.

VI. Discussion

The approaches in this work were aimed at wireless signal transmission out of a device with a minimum component space and power usage. The OCC methodology with the manually triggered transmissions by STELLA's hall sensor during routine animal health checks in conjunction with simultaneous OCC reception conserves implant battery capacity and requires a minimal setup. On the other hand it is limited in communication range and packet size.

Our second approach allows for arbitrary frame sizes and distances up to 1 m. Nevertheless, VLC is limited to line-of-sight applications. The viability of its usage in an autonomous monitoring scenario with freely moving animals, laterally positioned transmitter and potentially obstructed path between the LED and photodiode were an open question. The results of the trial have shown that about 1/4 of the transmissions could still be detected by the photodiode such that a 6 hour transmission interval should suffice for daily updates of the implant status on average.

The overall energy consumption depends on the payload size, the manually controlled transmission time for the OCC approach and the transmission interval for the second approach. However, with an average power consumption during transmissions of 2.8 mW for the PPM and 5.1 mW for the FSK modulation, our VLC solutions require 93% and 87% respectively less power compared to the RF module in [10] which is based on the same neurostimulator.

VII. Conclusion

In this case study, two approaches towards animal implant monitoring by VLC were investigated as an alternative to RF telemetry. Results have shown that both the triggered and autonomous approach are applicable to a scenario with freely moving animals. An advantage of the VLC approach compared to other technologies is the negligible amount of component space and cost of the implant itself. Moreover, the power consumption is significantly lower compared to typical RF telemetry.

Especially the low power consumption compared to RF telemetry makes it a viable solution for energy constraint applications.

Regarding the attempt to find biomarkers enabling closed-loop controlled stimulation, non-invasive data transfer may play a crucial role in the process realization.

Acknowledgment

This research was funded by the Deutsche Forschungsgemeinschaft (DFG, German Research Foundation) through the Collaborative Research Centre CRC 1270 'Electrically Active Implants' (DFG; SFB 1270/2–299150580).

References

[1] M. Jakobs, A. Fomenko, A. M. Lozano, and K. L. Kiening, "Cellular, molecular, and clinical mechanisms of action of deep brain stimulation-a systematic review on established indications and outlook on future developments," *EMBO molecular medicine*, vol. 11, no. 4, p. e9575, Apr. 2019.

[2] P. Krack, R. Martinez-Fernandez, M. Del Alamo, and J. A. Obeso, "Current applications and limitations of surgical treatments for movement disorders," *Movement Disorders: Official Journal of the Movement Disorder Society*, vol. 32, no. 1, pp. 36–52, Jan. 2017.

[3] C. Hamani and J. N. Nóbrega, "Deep brain stimulation in clinical trials and animal models of depression," *The European Journal of Neuroscience*, vol. 32, no. 7, pp. 1109–1117, Oct. 2010.

[4] K. Witt, C. Daniels, and J. Volkmann, "Factors associated with neuropsychiatric side effects after STN-DBS in Parkinson's disease," *Parkinsonism & Related Disorders*, vol. 18 Suppl 1, pp. S168–170, Jan. 2012.

[5] S. Alomar, N. K. K. King, J. Tam, A. A. Bari, C. Hamani, and A. M. Lozano, "Speech and language adverse effects after thalamotomy and deep brain stimulation in patients with movement disorders: A meta-analysis," *Movement Disorders: Official Journal of the Movement Disorder Society*, vol. 32, no. 1, pp. 53–63, Jan. 2017.

[6] S. G. J. Boccard, E. A. C. Pereira, and T. Z. Aziz, "Deep brain stimulation for chronic pain," *Journal of Clinical Neuroscience: Official Journal of the Neurosurgical Society of Australasia*, vol. 22, no. 10, pp. 1537–1543, Oct. 2015.

[7] F. Plocksties, M. Kober, C. Niemann, J. Heller, M. Fauser, M. Nüssel, F. Uster, D. Franz, M. Zwar, A. Lüttig, J. Kröger, J. Harloff, A. Schulz, A. Richter, R. Köhling, D. Timmermann, and A. Storch, "The software defined implantable modular platform (STELLA) for preclinical deep brain stimulation research in rodents," *Journal of Neural Engineering*, vol. 18, no. 5, p. 056032, Sep. 2021. [Online]. Available: https://doi.org/10.1088/1741-2552/ac23e1

[8] M. Fauser, M. Ricken, F. Markert, N. Weis, O. Schmitt, J. Gimsa, C. Winter, K. Badstübner-Meeske, and A. Storch, "Subthalamic nucleus deep brain stimulation induces sustained neurorestoration in the mesolimbic dopaminergic system in a Parkinson's disease model," *Neurobiology of Disease*, vol. 156, p. 105404, Aug. 2021.

[9] J. Jimenez-Shahed, "Device profile of the percept PC deep brain stimulation system for the treatment of Parkinson's disease and related disorders," *Expert Review of Medical Devices*, vol. 18, no. 4, pp. 319–332, Apr. 2021. [Online]. Available: https://doi.org/10.1080/17434440.2021.1909471

[10] F. Plocksties, O. U. Shah, F. Uster, M. Ali, M. Koschay, M. Kober, A. Storch, and D. Timmermann, "Energy-Efficient modular RF interface for fully implantable electrical devices in small rodents," in *2021 IEEE Biomedical Circuits and Systems Conference (BioCAS)*, Oct. 2021, pp. 1–6, iSSN: 2163-4025.

[11] C. Danakis, M. Afgani, G. Povey, I. Underwood, and H. Haas, "Using a CMOS camera sensor for visible light communication," in *2012 IEEE Globecom Workshops*, Dec. 2012, pp. 1244–1248, iSSN: 2166-0077.

[12] A. Duquel, R. Stanica, H. Rivano, and A. Desportes, "Decoding methods in LED-to-smartphone bidirectional communication for the IoT," in *2018 Global LIFI Congress (GLC)*. IEEE, feb 2018.

[13] H.-Y. Lee, H.-M. Lin, Y.-L. Wei, H.-I. Wu, H.-M. Tsai, and K. C.-J. Lin, "RollingLight," in *Proceedings of the 13th Annual International Conference on Mobile Systems, Applications, and Services*. ACM, may 2015.

[14] J. Ferrandiz-Lahuerta, D. Camps-Mur, and J. Paradells-Aspas, "A reliable asynchronous protocol for VLC communications based on the rolling shutter effect," in *2015 IEEE Global Communications Conference (GLOBECOM)*. IEEE, dec 2015.

[15] M. F. Ahmed, M. O. Ali, M. H. Rahman, and Y. M. Jang, "Real-time health monitoring system design based on optical camera communication," in *2021 International Conference on Information Networking (ICOIN)*, Jan. 2021, pp. 870–873, iSSN: 1976-7684.

[16] D. R. Dhatchayeny and Y. H. Chung, "Optical extra-body communication using smartphone cameras for human vital sign transmission," *Applied Optics*, vol. 58, no. 15, pp. 3995–3999, May 2019. [Online]. Available: https://opg.optica.org/ao/abstract.cfm?uri=ao-58-15-3995

[17] U. Dudko, K. Pflieger, and L. Overmeyer, "Optical autonomous sensor module communicating with a smartphone using its camera," in *Smart Photonic and Optoelectronic Integrated Circuits XXI*, E.-H. Lee and S. He, Eds. SPIE, mar 2019.

[18] C.-W. Chow, C.-Y. Chen, and S.-H. Chen, "Visible light communication using mobile-phone camera with data rate higher than frame rate," *Optics Express*, vol. 23, no. 20, pp. 26 080–26 085, Oct. 2015. [Online]. Available: https://opg.optica.org/oe/abstract.cfm?uri=oe-23-20-26080

[19] A. Viterbi, "Error bounds for convolutional codes and an asymptotically optimum decoding algorithm," *IEEE Transactions on Information Theory*, vol. 13, no. 2, pp. 260–269, 1967.